Optical and Quantum Electronics (2019)51:58
https://doi.org/10.1007/s11082-019-1772-5

Two-photon absorption in quantum dot semiconductor optical amplifiers-based all-optical XOR gate at 2 Tb/s

Amer Kotb[1,2] · **Chunlei Guo**[1,3]

Received: 8 June 2018 / Accepted: 4 February 2019
© Springer Science+Business Media, LLC, part of Springer Nature 2019

Abstract
The nonlinear effect of two-photon absorption (TPA) on the performance of all-optical XOR gate using quantum dot semiconductor optical amplifiers (QDSOAs)-assisted Mach–Zehnder interferometer is numerically analyzed and investigated at a data rate of 2 Tb/s. The dependence of the quality factor (QF) on the critical parameters of the input signal and QDSOA is examined and assessed. The obtained QFs for the all-optical XOR gate using QDSOAs-MZI at 2 Tb/s with TPA and without TPA are 14 and 8, respectively.

Keywords All-optical XOR gate · Two-photon absorption · Quantum dot semiconductor optical amplifier · Mach–Zehnder interferometer

1 Introduction

The nonlinearities of the optical fibers are weak. So, high power and long fiber are required to carry out the all-optical logic gates (AOLGs) which result in bulk size, increased latency, and limited energy efficiency. The required power is 1 W for a single-mode fiber of a length of 1 km. An alternative method to achieve the AOLGs is the nonlinearities offered by semiconductor optical amplifiers (SOAs). These nonlinearities are a magnitude stronger than fiber's, which significantly reduces the interaction lengths to millimeters (Patel et al. 1998). The most important SOA's advantages are the significant size reduction, which makes the switching devices compact and permits their integration, which further helps minimize their latency. The speed response of the gain and phase recovery times of the SOA are slow, which limit the speed of Boolean logic operations to < 100 Gb/s (Houbavlis et al. 2004; Sotoa et al. 2004; Dong et al. 2004, 2006a, b; Kim et al. 2005, 2006; Wang et al. 2006; Sun et al. 2006a, 2007a, b; Ye et al. 2006; Son et al. 2007; Kang et al. 2009; Kotb et al. 2011; Kotb and Maeda 2012; Saharia and Sharma 2014; Kotb 2016a, b, 2017; Kotb and Alamer 2016; Kotb and Zoiros 2016). These physical limitations can be overcome via

✉ Amer Kotb
amer@ciomp.ac.cn

[1] The Guo China-US Photonics Laboratory, Changchun Institute of Optics, Fine Mechanics, and Physics, Chinese Academy of Sciences, Changchun 130033, China

[2] Department of Physics, Faculty of Science, University of Fayoum, Fayoum 63514, Egypt

[3] The Institute of Optics, University of Rochester, Rochester, NY 14627, USA

two-photon absorption (TPA) nonlinear effect in SOA. The TPA of high intensities changes the amount of the carriers in the SOA's active media, which achieves a faster phase for a low-intensity beam. The performances of AOLGs based on TPA in SOAs at 250 Gb/s have been presented (Kotb et al. 2010a, b; Ma et al. 2009a, 2010a; Kotb 2013a, 2015a, b, 2016c; Kotb and Zoiros 2014a).

On the other hand, the gain recovery time of a quantum dots (QDs) placing in the active region of SOA is faster (i.e. 300 fs–10 ps), which improves the high-speed performances-based logic systems up to 1 Tb/s (Sun et al. 2005, 2006b, c; Ma et al. 2009b, 2010b; Dimitriadou and Zoiros 2012a, b, c, d; Kotb 2013a, b, 2015c, 2016d; Dimitriadou and Zoiros 2013a, b, c; Kotb and Zoiros 2013, 2014a, b). The gap between the QDs' levels and wetting layer (WL) results in shorter carrier relaxation times and lower gain saturation. In recent years, the QDSOAs provide a better device for signal processing in telecommunications systems. In this paper, we have combined the advantages of both QD and TPA to theoretically realize the performance of all-optical XOR gate at a data rate of 2 Tb/s. The fast phase recovery time due to TPA and the fast gain recovery time due to QD are required to achieve high-speed Boolean operations and hence a high output quality. The device used in this simulation work is the Mach–Zehnder interferometer (MZI), which has two symmetrical QDSOAs in its arms. The device has been named for physicists Ludwig Mach and Ludwig Zehnder around 1892 (Pereira et al. 2009). MZI is the most promising element due to its attractive features of strong nonlinearity, the potential for integration, high stability, low power consumption, and compactness. MZI has been fabricated with tilted waveguides to reduce the reflections at the facets and to couple the light to the semiconductor waveguides. The dependence of the QF on the key parameters of the input signal and the QDSOA has been theoretically studied. For realistic results, the impact of amplified spontaneous emission (ASE) has also been included. This simulation has been prepared and run via Mathematica Wolfram®.

This paper is organized as follows: The QDSOA-MZI modeling is formulated in Sect. 2. The operation principle and the results of the XOR operation are described in Sect. 3. Finally, Sect. 4 contains the concluding remarks.

2 QDSOA-MZI modeling

The semiconductor materials used in the QDSOAs device is the commonly employed InAs/GaAs, with InAs QDs embedded in a GaAs layer. The schematic of the QD with TPA's process is shown in Fig. 1. During the amplification process, the QDs' carriers that are depleted are refilled by carriers generated in the bulk region due to TPA on ultrafast timescales by carrier-relaxation via the wetting layer (WL).

In order to simulate the carrier densities and transitions that affect the QDSOA device gain dynamics, the QDs are assumed to be uniform and identical. Also, a two-level model is applied (Dutta and Wang 2013). In this model, the transitions resulting in photon emission take place from the QDs states conduction band to the valence band. Carriers produced in the WL via the injection current make the transition to the excited state, which acts as the carrier reservoir, followed by a transition to the ground state, which has ultrafast relaxation of carriers whose density determines the device gain.

The carrier heating (CH) results from carriers' thermalization in the entire energy band following the pulse. This process occurs on a time scale between 0.1 ps - 0.7 ps, which is very fast and can't be neglected. The pulse energy burns a hole in the gain spectrum

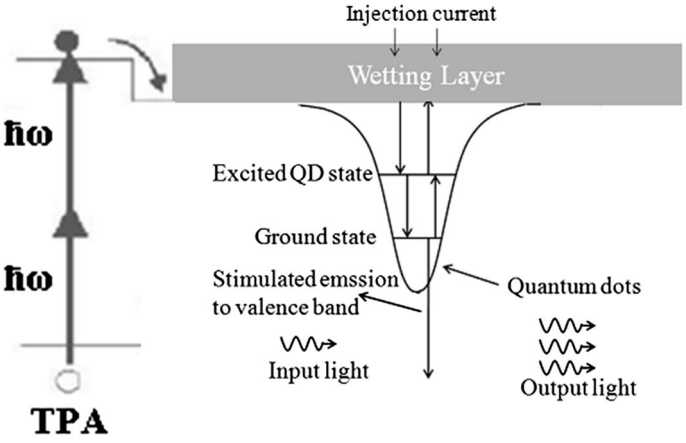

Fig. 1 Diagram of QDs' energy levels with TPA process

and produces a process known as spectral hole burning (SHB). By taking into account the interband and intraband effects the time-dependent gain of each QDSOA is described by the following coupled first-order differential equations (Kotb 2013c, d; Kotb and Zoiros 2013, 2014b, c):

$$\frac{dh_d(t)}{dt} = \frac{h_w(t)}{\tau_{dw}}\left(1 - \frac{h_d(t)}{h_0}\right) - \frac{h_d(t)}{\tau_{dr}} - \left(exp\left[h_d(t) + h_{CH}(t) + h_{SHB}(t)\right] - 1\right)\frac{Pin(t)}{E_{sat}} \tag{1}$$

$$\frac{dh_w(t)}{dt} = \frac{h_{in}}{\tau_{wr}}\left(1 - \frac{h_w(t)}{h_0}\right) - \frac{h_w(t)}{\tau_{wr}} - \frac{h_w(t)}{\tau_{wd}}\left(1 - \frac{h_d(t)}{h_0}\right) \tag{2}$$

$$\frac{dh_{CH}(t)}{dt} = \frac{h_{CH}(t)}{\tau_{CH}} - \frac{\varepsilon_{CH}}{\tau_{CH}}\left(exp\left[h_d(t) + h_{CH}(t) + h_{SHB}(t)\right] - 1\right)Pin(t) \tag{3}$$

$$\frac{dh_{SHB}(t)}{dt} = -\frac{h_{SHB}(t)}{\tau_{SHB}} - \frac{\varepsilon_{SHB}}{\tau_{SHB}}\left(exp\left[h_d(t) + h_{SHB}(t) + h_{CH}(t)\right] - 1\right)Pin(t) - \frac{dh_d(t)}{dt} - \frac{dh_{CH}(t)}{dt} \tag{4}$$

$$h_{in} = \int_0^z \frac{aJ\tau_{wr}}{ed}\,dz' \tag{5}$$

where function 'h' is the power gain of the QDSOA integrated over the longitudinal dimension, z, for carriers recombination between QDs states (h_d) and WL (h_w), carrier heating (h_{CH}), and spectral hole burning (h_{SHB}). $h_0 = \log[G_0]$, where G_0 is the unsaturated power gain, E_{sat} is the saturation energy, and Pin(t) is the input signal power. τ_{dw} is the excitation rate from QD ground state to WL and τ_{dr} is the recombination rate of QD. τ_{wd} is the transition rate from WL to QD ground state and τ_{wr} is the carrier recombination rate of WL. τ_{CH} and τ_{SHB} are the temperature relaxation rate and the carrier-carrier scattering rate, respectively. ε_{CH} and ε_{SHB} are the nonlinear gain suppression factors due to CH and SHB,

respectively. α is the differential gain, which represents the ratio of carriers in WL and QDs, J is the injection current density, d is the thickness of the WL, and e is the electron charge. The total phase of each QDSOA, including the TPA process is given by (Kotb 2013a, 2015a, b; Kotb and Zoiros 2014a):

$$\Phi(t) \;=\; -0.5\left(\alpha\, h\,(t) \;+\; \alpha_{CH} h_{CH}(t) + \beta\;\alpha_{TPA}\, L\, S(t)\right) \tag{6}$$

where α is the traditional linewidth enhancement factor (α-factor). α_{CH} and α_{SHB} are the linewidth enhancement factors due to CH and SHB, respectively. α_{TPA} is the linewidth enhancement factor due to TPA and β is the TPA coefficient. L is the length of the QDSOA active region and $S(t)$ is the photon density, which is linked to light power through the relevant conversion factor (Kotb et al. 2010a). The negative sign '−' means that the phase change due to TPA is in the opposite direction to the phase change due to QDSOA gain.

The input pulse powers (A & B) are assumed to be a Gaussian shape as described by:

$$P_{A,B}(t) \equiv P_{in}(t) = \sum_{n=1}^{N} a_{nA,B} \frac{2\sqrt{\ln(2)}\, E_0}{\sqrt{\pi}\, \tau_{FWHM}} \;\; exp\left[-\frac{4\ln(2)(t - n\,T)^2}{\tau_{FWHM}^2}\right] \tag{7}$$

where $a_{nA,B}$ represents the n-th pulse, which can take the logical value '1' or '0' of data 'A' or 'B'. E_0 is the input pulse energy, T is the bit period, and τ_{FWHM} is the pulse width (full-width at half-maximum). N is the length of the pseudorandom binary sequence (PRBS), which is $2^7 - 1$ bits-long (Dutta and Wang 2013).

The output power of the XOR operation is described by the following basic interferometric equation:

$$\begin{aligned} P_{XOR}(t) = \;& 0.25\, P_{CW}\big(G_{QDSOA1}(t) \;+\; G_{QDSOA2}(t) \\ & - 2\sqrt{G_{QDSOA1}(t)\, G_{QDSOA2}(t)}\; cos\left[\Phi_{QDSOA1}(t) - \Phi_{QDSOA2}(t)\right]\big) \end{aligned} \tag{8}$$

where P_{CW} is the CW power, $G_{1,2}(t)$ is the time-dependent gains, and $\Phi_{1,2}(t)$ is the phase shifts in the two arms of the QDSOA-MZI.

3 XOR

3.1 Operation principle

The schematic design and truth table of the all-optical XOR gate using QDSOAs-MZI is shown in Fig. 2.

For XOR operation, two modulated data signals A and B are inserted in QDSOA1 and QDSOA2, respectively. In parallel, a continuous wave (CW) beam is split by a 3 dB optical coupler (OC) into a pair of identical parts and is injected in the middle arm of the QDSOA-MZI. To combine the CW input with both data signals A and B, two reciprocal wavelength selective couplers (WSCs) are used. For A = '0' and B = '0', the MZI remains balanced and there is no output or equivalently the logical outcome is '0'. For A = '1', B = '0', the copy of the CW signal traveling in the upper MZI arm together with signal A suffers through cross-phase modulation a phase change versus its other split counterpart propagating in the lower MZI's arm. Thus, when these CW replicas recombine they interfere constructively, which results in output '1'. The same happens when A = '0' and B = '1'. However, when both A = '1' and B = '1', these CW constituents experience the same phase change,

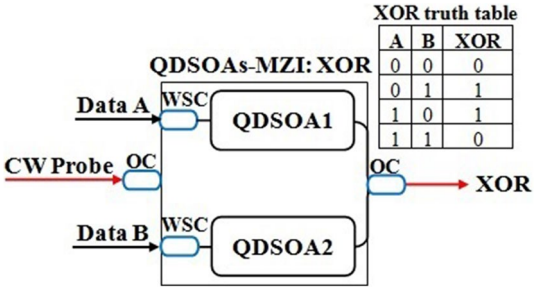

Fig. 2 Schematic design and truth table of XOR gate using QDSOAs-MZI. *OC 3 dB optical coupler*, *WSC* wavelength-selective coupler

so they interfere destructively and the output is '0'. In this manner, the XOR operation is executed between the binary content of A and B according to the truth table of this Boolean function.

3.2 Results

The performance of the all-optical XOR gate using QDSOA-MZI with TPA has been evaluated by the QF, which is defined as $QF=(P_1-P_0)/(\sigma_1+\sigma_2)$ (Dutta and Wang 2013), where P_1, P_0 are the average powers of the logical values '1's and '0's and σ_1, σ_2 are the standard deviations of those powers. The symbol, definition, and value of the key parameters used in this simulation have been cited in Table 1.

Figures 3 and 4 show the simulation results and eye diagrams for the all-optical XOR operation using QDSOAs-MZI at 2 Tb/s without and with TPA, respectively. These results show that owing to TPA it is possible to realize the specific Boolean operation with both pattern-free logical correctness and higher QF than without TPA.

The saturation energy (E_{sat}) of the amplifier is related to the optical confinement factor (Γ) by the following relation (Dutta and Wang 2013):

$$E_{sat} = \frac{h\,\omega_0\,\sigma_m}{a_N\,\Gamma} \tag{9}$$

where h is Planck's constant and ω_0 is the centered frequency. σ_m is the cross-section of the active region, which is defined by $\sigma_m \cong wd$ (w and d are the width and thickness of the active layer). a_N is the device's differential gain coefficient with a value of $8.9\times10^{-15}\text{cm}^{-2}$ for a QDSOA (Berg et al. 2001). The value of a_N is small in QDSOAs to improve the saturation characteristics. Figure 5 shows the dependence of the QF on the confinement factor (Γ) and the saturation power (P_{sat}) for XOR gate using QDSOA-MZI with and without TPA at 2 Tb/s. At low Γ, the output signal is degraded and also the QF as shown in Fig. 5a. The similar trend is observed in Fig. 5b, where the QF against the QDSOA's saturation power. This figure confirms that the QF inclines with increasing the saturation power. The TPA reduces the pattern effects and results in a higher QF.

The QF as a function of the energy and width of the input pulse for XOR operation with and without TPA using QDSOAs-MZI at 2 Tb/s is calculated as shown in Fig. 6a, b, respectively. Without TPA, a high energetic pulse depletes the carrier density via the stimulated emission, which needs a longer time to recover to its initial level. This causes a stronger pattern effect and degrades the QF as shown in Fig. 6a. On the other hand, with TPA, the carrier density is depleted by high energetic pulses recovers faster owing

Table 1 Critical parameters calculation values

Symbol	Definition	Value	Unit
E_0	Pulse energy	0.01	pJ
τ_{FWHM}	Pulse width	0.2	ps
T	Bit period	0.5	ps
N	PRBS' length	127	–
λ_A	Wavelength of data A	1550	nm
λ_B	Wavelength of data B	1556	nm
β	TPA coefficient	30	cm/GW
α_{TPA}	TPA linewidth enhancement factor	−4	–
J	Injection current density	50	kA/cm^2
P_{sat}	Saturation power	30	mW
τ_{wd}	Transition rate from WL to QDs state	5	ps
τ_{dw}	Excitation rate from QDs state to WL	10	ns
τ_{wr}	Carrier recombination rate in WL	2.2	ns
τ_{dr}	Carrier recombination rate in QDs state	0.4	ns
τ_{CH}	Temperature relaxation rate	0.3	ps
τ_{SHB}	Carrier-carrier scattering rate	0.1	ps
α	Traditional α-factor	4	–
α_{CH}	CH linewidth enhancement factor	1	–
α_{SHB}	SHB linewidth enhancement factor	0	–
ε_{CH}	CH nonlinear gain suppression factor	0.02	W^{-1}
ε_{SHB}	SHB nonlinear gain suppression factor	0.02	W^{-1}
Γ	Confinement factor	0.15	–
a	Differential gain	8.6×10^{-15}	cm^{-2}
d	WL thickness	0.5	μm
L	Length of QDSOA active region	1.0	mm
G_0	Unsaturated power gain	30	mm
N_{SP}	Spontaneous emission factor	2	–

to the TPA-induced extra carriers offered via the WL. Similarly and as shown in Fig. 6b, the QF is decreased for broader pulses of fixed energy. Still, the QF is more acceptable with TPA than without TPA.

The dependence of the QF on the injection current density and the transition rate from WL to QD ground state (τ_{wd}), with and without TPA, using QDSOAs-MZI at 2 Tb/s is shown in Fig. 7a, b, respectively. The carrier density is increased via the carriers injected into the WL by the injection current. The QF is increased for higher injection current density as shown in Fig. 7a. On the other hand, the dynamic gain process is accelerated for short τ_{wd}, so the QF is improved for smaller values of this parameter as shown in Fig. 7b and is much more when the TPA is presented.

Figure 8 shows the QF versus the length and thickness of the active region of the QDSOA for XOR operation with and without TPA at 2 Tb/s. Generally, the QF is high for the longer and thicker active region. The optical gain region is determined by the width of the active region. A wide active region increases the carrier density, which results in a high QF. these figures confirm that the performance of the considered Boolean function is more acceptable with TPA than without TPA.

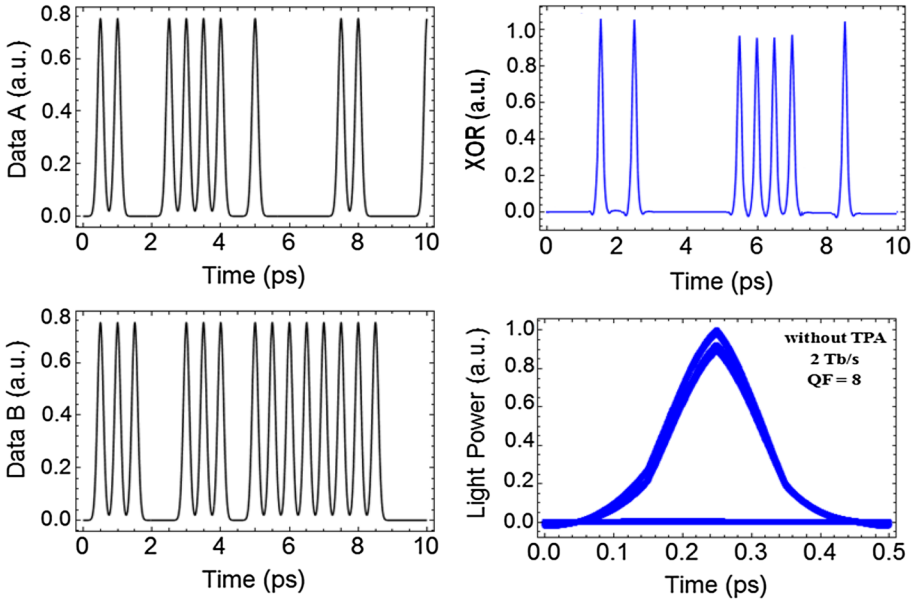

Fig. 3 Simulation results for XOR operation without TPA using QDSOAs-MZI at 2 Tb/s

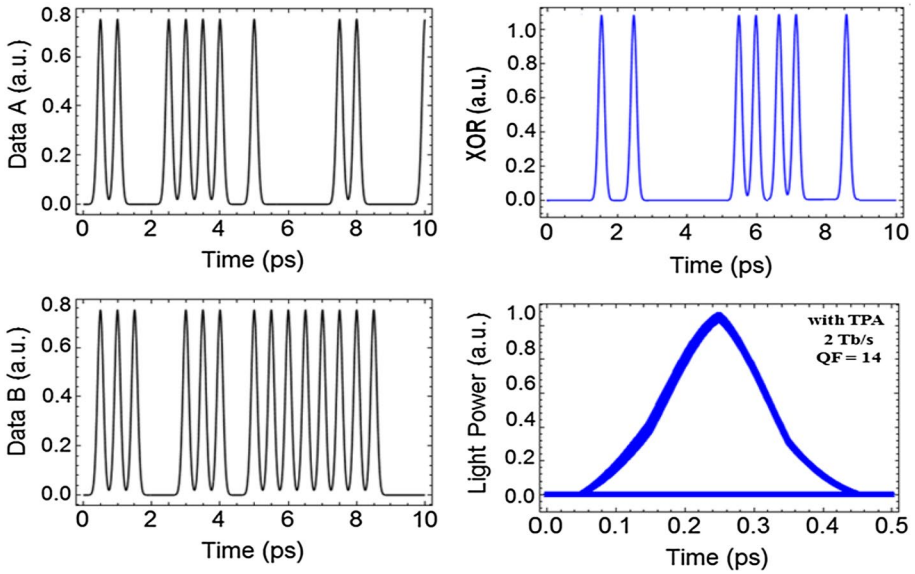

Fig. 4 Simulation results for XOR operation without TPA using QDSOAs-MZI at 2 Tb/s

The amplified spontaneous emission (ASE) is generated by the emission of the spontaneous photons and amplified through the amplifier medium to cause additional noise. A larger ASE noise increases the average intensity of the pulse of '0' level and hence reduces the QF.

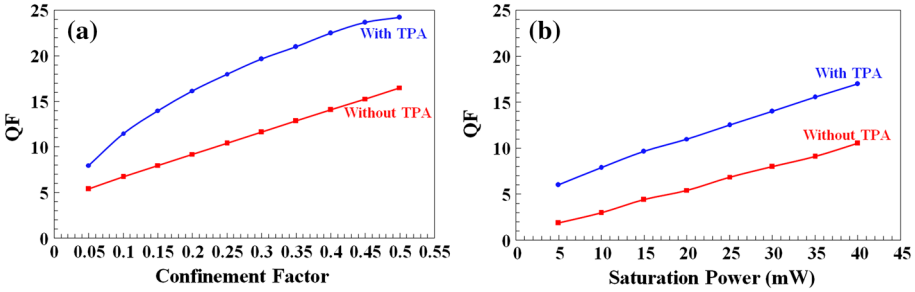

Fig. 5 QF versus **a** confinement factor and **b** saturation power for XOR operation using QDSOA-MZI with TPA and without TPA at 2 Tb/s

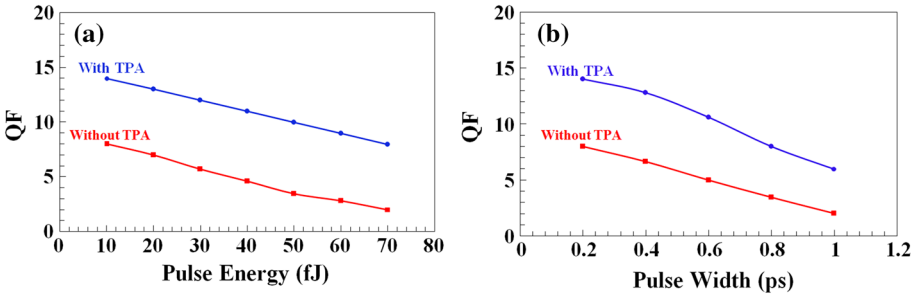

Fig. 6 QF versus **a** pulse energy and **b** pulse width for XOR operation using QDSOAs-MZI with and without TPA at 2 Tb/s

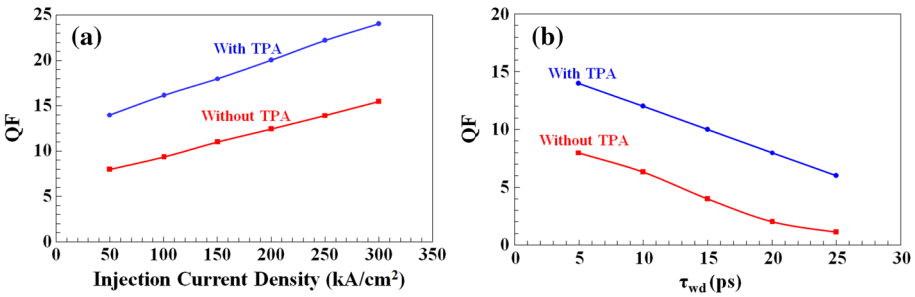

Fig. 7 QF versus **a** injection current density and **b** transition rate from WL to QDs ground state (τ_{wd}) for QDSOAs-based XOR operation at 2 Tb/s with and without TPA

The ASE is related to the spontaneous emission factor (N_{sp}) by the following relation (Kotb et al. 2011):

$$P_{ASE} = N_{sp}(G_0 - 1)\, h\, \upsilon B_0 \tag{10}$$

where h is Planck's constant, G_0 is the unsaturated power gain, and B_0 is the optical bandwidth at an optical frequency (υ). The noise effect on the QF is accounted for

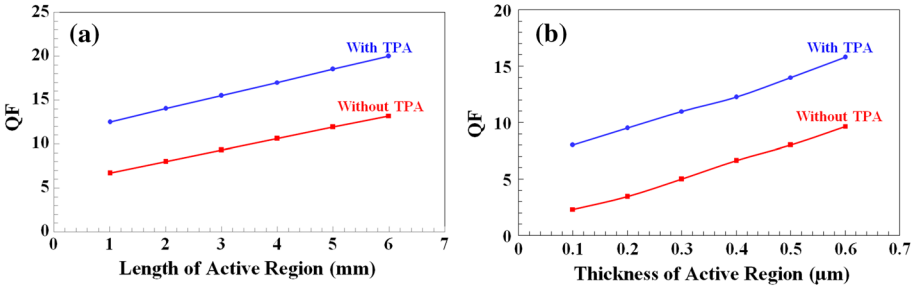

Fig. 8 QF versus **a** length and **b** thickness of active region of QDSOAs for XOR operation at 2 Tb/s with and without TPA

Fig. 9 QF versus spontaneous emission factor (N_{sp}) for XOR operation using QDSOAs-MZI at 2 Tb/s with and without TPA

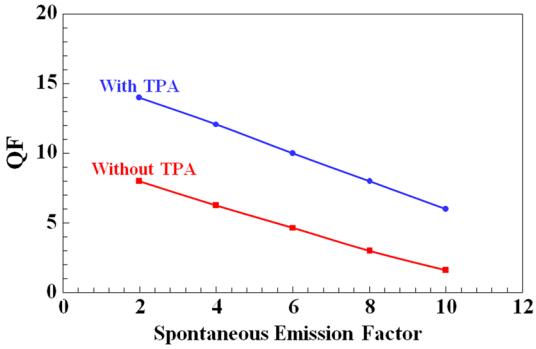

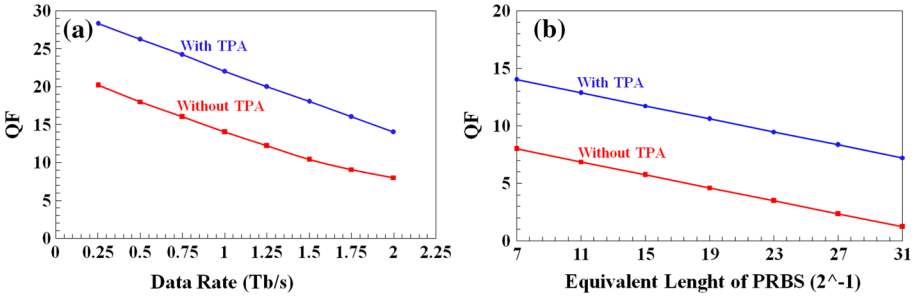

Fig. 10 QF versus **a** data rate and **b** equivalent length of PRBS for XOR operation using QDSOAs-MZI at 2 Tb/s with and without TPA

by numerically adding the ASE power to the XOR output power. The parameters used to obtain this figure are $B_0 = 3$ nm and $\lambda = 1550$ nm. The achieved QFs at $N_{sp} = 2$ for the all-optical XOR operation using QDSOAs-MZI are 14 and 8 with TPA and without TPA, respectively. The QF is decreased with increasing N_{sp} as shown in Fig. 9.

The QF versus the data rate and equivalent length of the PRBS for the QDSOA-based XOR operation with and without TPA as shown in Fig. 10a, b, respectively. The QF is decreased with the increase of the data rate as shown in Fig. 10a. The QF remains higher and more acceptable in the presence of the TPA. A similar trend is observed when the QF

against the equivalent length of the PRBS. Figure 10b shows that the operation of the XOR gate is affected by the higher equivalent lengths of the PRBS carried by each input data. Despite the increased strain imposed by longer PRBS, the scheme is tolerant to this effect and retains its acceptable performance when applying the TPA.

4 Conclusion

The performance of all-optical XOR gate when taking into account the nonlinear effect of the two-photon absorption (TPA) in quantum dot semiconductor optical amplifiers (QDSOAs)-assisted Mach–Zehnder interferometer (MZI) was numerically analyzed and investigated at a data rate of 2 Tb/s. The dependence of the quality factor on the key parameters of the input signal and QDSOA was examined and assessed. The main conclusion of this study is that including TPA is more efficient for realizing the performance of the all-optical XOR operation using QDSOAs-MZI at 2 Tb/s than when using QDSOAs-MZI without TPA.

Acknowledgements This work was funded by Chinese Academy of Sciences President's International Fellowship Initiative (PIFI) (Grant No. 2019FYT0002) and Talented Young Scientist Program (TYSP) supported by China Science and Technology Exchange Center of Ministry of Science and Technology of China.

References

Berg, T., Bischoff, S., Magnusdottir, I., Mork, J.: Ultrafast gain recovery and modulation limitations in self-assembled quantum-dot devices. IEEE Photon. Technol. Letts. **13**, 541–543 (2001)

Dimitriadou, E., Zoiros, K.E.: On the design of reconfigurable ultrafast all-optical NOR and NAND gates using a single quantum-dot semiconductor optical amplifier-based Mach–Zehnder interferometer. J. Opt. **14**(105401), 1–9 (2012a)

Dimitriadou, E., Zoiros, K.E.: On the design of ultrafast all-optical NOT gate using quantum-dot semiconductor optical amplifier-based Mach–Zehnder interferometer. Opt. Laser Technol. **44**, 600–607 (2012b)

Dimitriadou, E., Zoiros, K.E.: Proposal for all-optical NOR gate using single quantum-dot semiconductor optical amplifier-based Mach–Zehnder interferometer. Opt. Commun. **285**, 1710–1716 (2012c)

Dimitriadou, E., Zoiros, K.E.: On the feasibility of ultrafast all-optical NAND gate using single quantum-dot semiconductor optical amplifier-based Mach–Zehnder interferometer. Opt. Laser Technol. **44**, 1971–1981 (2012d)

Dimitriadou, E., Zoiros, K.E.: All-optical XOR gate using single quantum-dot SOA and optical filter. Lightwave Technol. **31**, 3813–3821 (2013a)

Dimitriadou, E., Zoiros, K.E.: On the feasibility of 320 Gb/s all-optical AND gate using quantum-dot semiconductor optical amplifier-based Mach–Zehnder interferometer. Prog. Electromagn. Res. B (PIERS) **50**, 113–140 (2013b)

Dimitriadou, E., Zoiros, K.E.: Proposal for ultrafast all-optical XNOR gate using single quantum-dot semiconductor optical amplifier-based Mach–Zehnder interferometer. Opt. Laser Technol. **45**, 79–88 (2013c)

Dong, H., Wang, Q., Zhu, G., Jaques, J., Piccirilli, A.B., Dutta, N.K.: Demonstration of all-optical OR gate using semiconductor optical amplifier-delayed interferometer. Opt. Commun. **242**, 479–485 (2004)

Dong, H., Sun, H., Wang, Q., Dutta, N.K., Jaques, J.: 80 Gb/s all-optical logic AND operation using Mach–Zehnder interferometer with differential scheme. Opt. Commun. **265**, 79–83 (2006a)

Dong, H., Sun, H., Wang, Q., Dutta, N.K., Jaques, J.: All-optical logic AND operation at 80 Gb/s using Semiconductor optical amplifier based Mach–Zehnder interferometer. Microw. Opt. Technol. Lett. **48**, 1672–1675 (2006b)

Dutta, N.K., Wang, Q.: Semiconductor Optical Amplifiers, 2nd edn. World Scientific Publishing Company, Singapore (2013)
Houbavlis, T., Zoiros, K.E., Kanellos, G., Tsekrekos, C.: Performance analysis of ultrafast all-optical Boolean XOR gate using semiconductor optical amplifier-based Mach–Zehnder interferometer. Opt. Commun. **232**, 179–199 (2004)
Kang, I., Rasras, M., Buhl, L., Dinu, M., Cabot, S., Cappuzzo, M., Gomez, L.T., Chen, Y.F., Patel, S.S., Dutta, N., Piccirilli, A., Jaques, J., Giles, C.R.: All-optical XOR and XNOR operations at 86.4 Gb/s using a pair of semiconductor optical amplifier Mach-Zehnder interferometers. Opt. Express **17**, 19062–19066 (2009)
Kim, S.H., Kim, J.H., Choi, J., Woo, D.H.: All-optical NAND gate using cross-gain modulation in semiconductor optical amplifiers. Electron. Lett. **2**, 957–959 (2005)
Kim, J.Y., Kang, J.M., Kim, T.Y., Han, S.K.: All-optical multiple logic gates with XOR, NOR, OR and NAND functions using parallel SOA-MZI structures: theory and experiment. Lightwave Technol. **24**, 3392–3399 (2006)
Kotb, A.: AND based on two-photon absorption in semiconductor optical amplifier. Optoelectron. Letts. **9**, 181–184 (2013a)
Kotb, A.: NAND gate with quantum-dot semiconductor optical amplifiers-based Mach–Zehnder interferometer. Optoelectron. Letts. **9**, 89–92 (2013b)
Kotb, A.: NOR gate based on QD-SOA at 250 Gbit/s. Opt. Quantum Electron. **45**, 473–480 (2013c)
Kotb, A.: 1 Tb/s high-quality factor NOR gate based on quantum-dot semiconductor optical amplifier. Op. Quantum Electron. **45**, 1258–1268 (2013d)
Kotb, A.: Performance of all-optical XNOR gate based on two-photon absorption in semiconductor optical amplifiers. Adv. Opt. Technol. **2014**, 754713 (2015a)
Kotb, A.: Simulation of all-optical logic NOR gate based on two-photon absorption with semiconductor optical amplifier-assisted Mach–Zehnder interferometer with the effect of amplified spontaneous emission. Korean Phys. Soc. **66**, 1593–1598 (2015b)
Kotb, A.: Modeling of high-quality-factor XNOR gate using quantum-dot semiconductor optical amplifiers at 1 Tb/s. Braz. J. Phys. **45**, 288–295 (2015c)
Kotb, A.: Simulation of soliton all-optical logic XOR gate with semiconductor optical amplifier. Opt. Quantum Electron. **48**(307), 1–11 (2016a)
Kotb, A.: Numerically simulation of soliton OR gate with semiconductor optical amplifier-assisted delayed interferometer. Opt. Quantum Electron. **48**(462), 1–12 (2016b)
Kotb, A.: Ultrafast all-optical logic OR gate based on two-photon absorption with a semiconductor optical amplifier-assisted delayed interferometer. Korean Phys. Soc. **68**, 201–205 (2016c)
Kotb, A.: Simulation of high-quality-factor all-optical logic gates based on quantum-dot semiconductor optical amplifier at 1 Tb/s. Optik **126**, 320–325 (2016d)
Kotb, A.: Theoretical analysis of soliton NOR gate with semiconductor optical amplifier-assisted Mach–Zehnder interferometer. Opt. Quantum Electron. **49**(180), 1–11 (2017)
Kotb, A., Alamer, F.A.: Dispersion on all-optical logic XOR gate using semiconductor optical amplifier. Opt. Quantum Electron. **48**(327), 1–10 (2016)
Kotb, A., Maeda, J.: All-optical logic NXOR based on semiconductor optical amplifiers with the effect of amplified spontaneous emission. Optoelectron. Lett. **8**, 437–440 (2012)
Kotb, A., Zoiros, K.E.: Simulation of all-optical logic XNOR gate based on quantum- dot semiconductor optical amplifiers with amplified spontaneous emission. Opt. Quantum Electron. **45**, 1213–1221 (2013)
Kotb, A., Zoiros, K.E.: Performance of all-optical XOR gate based on two-photon absorption in semiconductor optical amplifier-assisted Mach–Zehnder interferometer with effect of amplified spontaneous emission. Opt. Quantum Electron. **46**, 935–944 (2014a)
Kotb, A., Zoiros, K.E.: On the design of all-optical gates based on quantum-dot semiconductor optical amplifier with effect of amplified spontaneous emission. Opt. Quantum Electron. **46**, 977–989 (2014b)
Kotb, A., Zoiros, K.E.: 1 Tb/s high-quality factor NAND gate using quantum-dot semiconductor optical amplifiers in Mach–Zehnder interferometer". Comput. Electron. **13**, 555–561 (2014c)
Kotb, A., Zoiros, K.E.: Soliton all-optical logic AND gate with semiconductor optical amplifier-assisted Mach–Zehnder interferometer. Opt. Eng. **55**(087109), 1–7 (2016)
Kotb, A., Ma, S., Chen, Z., Dutta, N.K., Said, G.: All-optical logic NAND based on two-photon absorption in semiconductor optical amplifiers. Opt. Commun. **283**, 4707–4712 (2010a)
Kotb, A., Ma, S., Chen, Z., Dutta, N.K., Said, G.: All-optical logic NAND based on two-photon absorption. SPIE Photonic Devices + Applications **7**, 77810D (2010b)

Kotb, A., Ma, S., Chen, Z., Dutta, N.K., Said, G.: Effect of amplified spontaneous emission on semiconductor optical amplifier based all-optical logic. Opt. Commun. **284**, 5798–5803 (2011)
Ma, S., Chen, Z., Dutta, N.K.: All-optical logic gates based on two-photon absorption in semiconductor optical amplifiers. Opt. Commun. **282**, 4508–4512 (2009a)
Ma, S., Sun, H., Chen, Z., Dutta, N.K.: High-speed all-optical PRBS generation based on quantum-dot semiconductor optical amplifiers. Opt. Express **17**(21), 18469–18477 (2009b)
Ma, S., Kotb, A., Chen, Z., Dutta, N.K.: All-optical logic gates based on two-photon absorption. Proc. SPIE **7750**, 77501L (2010a)
Ma, S., Chen, Z., Sun, H., Dutta, N.K.: High-speed all-optical logic gates based on quantum-dot semiconductor optical amplifiers. Opt. Express **18**, 6417–6422 (2010b)
Patel, N.S., Hall, K.L., Rauschenbach, K.A.: Interferometric all-optical switches for ultrafast signal processing. Appl. Opt. **37**, 2831–2842 (1998)
Pereira, A., Ostermann, F., Cavalcanti, C.: On the use of a virtual Mach–Zehnder interferometer in the teaching of quantum mechanics. Phys. Educ. **44**, 281–291 (2009)
Saharia, A., Sharma, R.: An approach for Realization of all-optical NAND gate using the nonlinear effect in SOA. Int. J. Signal Process. Imaging Eng. **1**, 13–17 (2014)
Son, C.W., Kim, S.H., Jhon, Y.M., Byun, Y.T., Lee, S., Woo, D.H., Kim, S.K., Yoon, T.H.: Realization of all-optical XOR, NOR, and NAND gates in a single format by using semiconductor optical amplifiers. Jpn. J. Appl. Phys. **46**, 232–234 (2007)
Sotoa, H., Alvareza, E., Dıaz, C.A., Topomondzo, J., Erasmeb, D., Schares, L., Occhi, L., Guekos, G., Castro, M.: Design of an all-optical NOT XOR gate based on cross-polarization modulation in a semiconductor optical amplifier. Opt. Commun. **237**, 121–131 (2004)
Sun, H., Wang, Q., Dong, H., Dutta, N.K.: XOR performance of a quantum-dot semiconductor optical amplifier based Mach–Zehnder interferometer. Opt. Express **13**, 1892–1899 (2005)
Sun, H., Wang, Q., Dong, H., Dutta, N.K., Jaques, J., Piccirilli, A.B.: All-optical logic XOR gate using SOA-MZI-DI. IEEE J. Quantum Electron. **42**, 747–781 (2006a)
Sun, H., Wang, Q., Dong, H., Dutta, N.K.: All-optical logic performance of quantum-dot semiconductor amplifier-based devices. Microw Opt. Technol. Letts. **48**, 29–35 (2006b)
Sun, H., Dong, H., Wang. Q., Dutta, N.K.: All-optical logic performance of quantum dot semiconductor amplifier-based devices. Proc. SPIE **6115**, 61151H (2006c)
Sun, H., Chen, Z., Ma, S., Dutta, N.K.: 80 Gb/s all-optical XNOR using four-wave mixing in highly nonlinear fibers. Proc. SPIE **6775**, 67750A (2007a)
Sun, H., Chen, Z., Ma, S., Dutta, N.K.: All-optical logic NOR gate at 40 Gb/s using SOA-based Mach–Zehnder interferometer. Proc. SPIE **6775**, 67750F (2007b)
Wang, Q., Dong, H., Sun, H., Dutta, N.K.: All-optical logic OR gate using SOA delayed Interferometer. Opt. Commun. **260**, 81–86 (2006)
Ye, X., Ye, P., Zhang, M.: All-optical NAND gate using integrated SOA-based Mach–Zehnder interferometer. Opt. Fiber Technol **12**, 312–316 (2006)

Publisher's Note Springer Nature remains neutral with regard to jurisdictional claims in published maps and institutional affiliations.